Observation of ferroelectric domain structures by secondary-electron microscopy in as-grown $KTiOPO_4$ crystals

G. Rosenman,* A. Skliar, and I. Lareah
Department of Electrical Engineering-Physical Electronics, Tel Aviv University, Ramat Aviv, 69978, Israel

N. Angert
Raicol Crystals Ltd, POB 3, Ariel, 44837, Israel

M. Tseitlin
The Research Institute, The College of Judea and Samaria, POB 3, Ariel, 44837, Israel

M. Roth
School of Applied Science and Technology, The Hebrew University of Jerusalem, Jerusalem, 91904, Israel
(Received 1 February 1996)

Ferroelectric domain structures of as-grown $KTiOPO_4$ crystals are observed on polished polar surfaces by the scanning secondary-electron microscopy (SEM) method. The results demonstrate a different contrast origin for domain boundaries and domains themselves. It is shown that the electron-beam irradiation in SEM causes a local heating of the ferroelectric crystal. Detailed calculations of the effects involved allow to assume that pyroelectric potentials induced by heating are opposite in sign for C^+ and C^- domains which is the main reason for the domain contrast. Domain boundaries are revealed due to the converse piezoelectric effect and the corresponding crystal deformations of ferroelectric domains are induced by electron-beam charging. [S0163-1829(96)05933-4]

I. INTRODUCTION

Potassium titanyle phosphate $KTiOPO_4$ (KTP) crystals exhibit excellent nonlinear optical properties making them attractive for frequency doubling by second-harmonic generation (SHG) and optical parametric oscillations.[1,2] Besides numerous bulk devices, the development of KTP-based nonlinear optical waveguides has greatly broadened the spectrum of applications of this material. Quasiphase matching between the fundamental frequency and second harmonic in waveguides has been achieved by periodic spontaneous polarization reversal.[3] Thus obtained domain grating in KTP has allowed us to build a compact blue laser with output power as high as 3.6 mW.[4] The most critical point in the laser fabrication is a ferroelectric domain structure control both for virgin and for domain grated crystals.

Ferroelectric domain structures may be observed by different methods[5] including polarizing microscope technique, etching, powder deposition methods, secondary-electron microscopy, and scanning force microscopy.[6] Several techniques have been also developed for domains observation in KTP crystals.[7–10] They are based on piezoelectric,[7] electro-optic,[7,9] nonlinear optical, and pyroelectric properties[7,8] of this ferroelectric material. The domains of KTP crystals have been also decorated on cleaved polar surfaces by using nematic liquid crystals.[9] Selective etching of domains with opposite directions of spontaneous polarization P_s was utilized for optical and electron microscopy studies including scanning electron microscopy.[9] Recently,[11] the domain grating formation in KTP have been controlled by means of the SHG method. In this paper we report on *in situ* observation of the KTP ferroelectric domain structure using a scanning secondary-electron microscope.

II. STUDIED CRYSTALS AND EXPERIMENTAL TECHNIQUE

Specimens of Z-cut plates (1 mm thick) were made from a $\langle 100 \rangle$ pyramid of KTP crystal grown by the flux method.[10] The preliminary domain mapping was performed by two conventional methods: optical microscopy of etched samples and piezoelectric probing. Etching was carried out using the mixture of KOH and KNO_3 solutions according to the method developed in Ref. 8. It is known that the etching is selective for domains with opposite directions of the polar axis. The piezoelectric domain mapping was done by measuring of the electric response induced by a force needle head due to pulsed compressing a polar KTP C surface.[8] It is known that the sign of the piezoelectric coefficient d_{33} and, consequently, of the detected piezoelectric signal depends on a domain orientation.

KTP samples characterized by the method described above were subsequently investigated by using the model ''JEOL JSM-6300'' scanning electron microscope equipped with the ''Oxford Instruments'' software program. The studied polar surfaces were polished and uncoated. The TV mode electron scanning regime was used in the frame time (40 ms). Crystals were studied in the secondary emission mode only. All data were obtained under the following parameters: electron probe current $J=1.5\times10^{-8}$ A, magnification $\times 55$. The SEM images were observed by variation of the primary electron-beam energy $E_{\rm pr}$ in the range 0.2–4 keV and they were treated by using the ''Aldus PhotoStyler 2.0'' software.

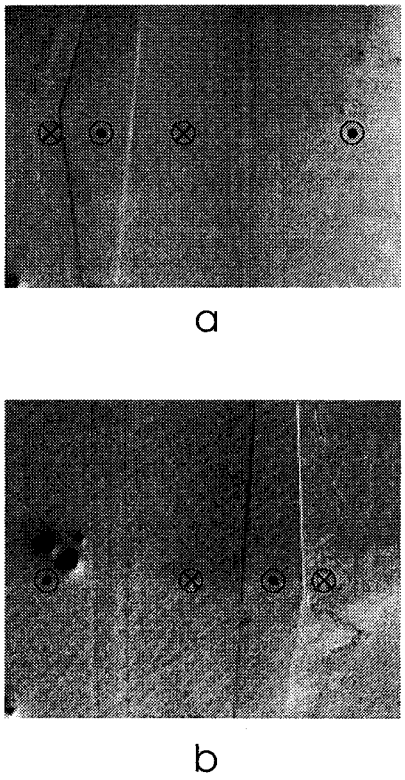

FIG. 1. Domain boundaries SEM contrast for Z-cut as-grown KTP crystal (energy of primary electrons $E_{pr}=2.8$ keV, $\times 55$). The ''b'' image was obtained for the sample turned around Z axis by 180°. $\odot$ indicates C^+ domains, $\otimes$ indicates C^- domains.

The conductivity of KTP samples was measured using the Keithley 617 programmable electrometer. Measurements of the work function for C^+ and C^- domains were implemented by the Kelvin probe method.

III. EXPERIMENTAL RESULTS

Spontaneous ferroelectric polarization maps of the virgin domain structure of KTP crystals have been obtained using the selective character of KTP etching. C^- domains react with etchant, while C^+ domains do not. The domain structure of some samples was also studied by the piezoelectric probing. Both methods showed identical results. These measurements allow us to choose for the SEM studies specific areas of KTP samples containing large C^+ and C^- single domains as well as multidomain structure.

Figures 1(a) and 1(b) show the SEM image of the central part of a typical KTP sample ($E_{pr}=2.8$ keV). A triangular C^+ domain surrounded by C^- domains and a multidomain region can be distinguished due to the appearance of domain boundaries only. However there is no contrast between domains with different orientation of $\mathbf{P}_s$. It should be noted that the domain boundaries appear as ''dark'' and ''bright'' lines on the opposite sides of the domains. This contrast direction depends on the sample orientation. When the sample is turned around the Z axis by 180° the contrast gets fully inverted: all previously ''dark'' boundaries become ''bright'' and ''bright'' boundaries are converted to ''dark'' [Fig. 1(b)]. The presented SEM images [Figs. 1(a) and 1(b)]

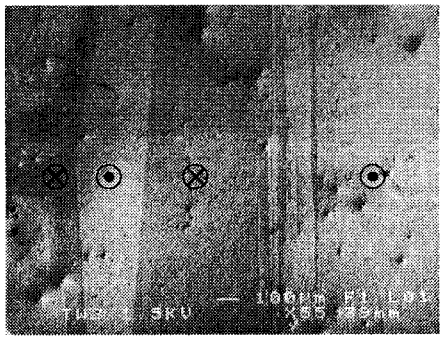

FIG. 2. Domain contrast for Z-cut KTP crystal ($E_{pr}=1.5$ keV, $\times 55$). $\odot$ indicates C^+ domains, $\otimes$ indicates C^- domains.

have been observed within a fairly narrow acceleration voltage range, 2.1 keV$\leqslant E_{pr}\leqslant$4.0 keV. The strongest domain boundary contrast occurs at 2.3 keV$\leqslant E_{pr}\leqslant$3.0 keV. Primary electron-beam energy E_{pr} increase ($E_{pr}\geqslant$3.0 keV) causes a reduction of contrast. At voltage $E_{pr}\geqslant$4.0 keV the SEM image of the domain boundaries disappears completely and no details of the domain structure can be observed.

Quite different SEM images have been obtained at $E_{pr}\leqslant$2.0 keV (Fig. 2). The gradually reduced domain boundary contrast is turned, also gradually, into the domain contrast when the accelerated voltage is decreased. The SEM image demonstrated in Fig. 2 shows that the C^+ domains are bright and C^- domains are dark.

The measured conductivity of KTP crystals along the spontaneous polarization direction is $\sigma_z\approx 10^{-8}\ \Omega^{-1}\mathrm{cm}^{-1}$, and for other directions $\sigma_y=\sigma_x\approx 10^{-11}\ \Omega^{-1}\mathrm{cm}^{-1}$. The work functions for the domains with opposite directions of $\mathbf{P}_s$ have been found to be equal, $A_{C^+}=A_{C^-}=4.5$ eV.

IV. ELECTRON PROCESSES IN KTP CRYSTALS CAUSED BY ELECTRON IRRADIATION

Comparison between optical microscopy and SEM images (Figs. 1 and 2) of the studied KTP crystals demonstrates a complete identity of the revealed domain configurations. Two kinds of contrast have been observed. The first one is the domain boundary contrast (Fig. 1) and the second one is difference in the brightness between C^+ and C^- domains (Fig. 2).

The origin of the domain contrast for numerous ferroelectric crystals was studied previously.[12–17] The great advantage of the results[12–17] is that they have been obtained on unmetallized surfaces as originally proposed in Refs. 12 and 13. The authors[12–17] have attributed the SEM domain contrast mainly to the electric field of spontaneous polarization, namely to the difference in work functions of domains with opposite polarization and to the ''charging'' effect. Obviously, the observed domain contrast in the used secondary-electron emission mode (Fig. 2) occurs due to the different secondary-electron currents from domains with opposite directions of spontaneous polarization. The experimental results (Fig. 2) show that the C^+ domains are sufficiently brighter than the C^- domains. It means that the secondary-electron emission yield (current) J_{C^+} is larger than J_{C^-}.

Two factors may influence the currents of the secondary electrons: asymmetric flux of secondaries along and opposite

polar axis $\mathbf{P}_s$ and changes of the work function of the opposite domains caused by the electron irradiation. Ferroelectrics are crystals without a center of symmetry. Elementary-electron processes for them are asymmetric for nonthermalized carriers of charge.[20,21] For instance, light illumination of ferroelectrics excites photoelectrons in the lattice and direct ''photovoltaic'' current is observed along the polar axis $\mathbf{P}_s$.[20,21] The primary electron beam leads to the appearance of secondary nonthermalized electrons with energies $E \gg kT$.[18,19] One can assume that an asymmetric electron flux of secondary electrons should be observed. It means that the secondary emission current from C^+ domains may be larger than from C^-: $J_{C^+} > J_{C^-}$. Another contribution to the observed difference in the secondary-electron emission currents from C^+ and C^- domains are possible changes of the work function of the domains originating from electrostatic charges induced by the primary electron-beam irradiation.

V. CHARGES AND POTENTIALS OF IRRADIATED FERROELECTRIC KTP CRYSTALS

Irradiation in SEM of any dielectric causes a sample charging if the secondary-electron emission coefficient $\delta \neq 1$. The positive charge $\Delta\rho$ at an irradiated surface appears for $\delta > 1$ and the negative one for $\delta < 1$. The corresponding changes of the surface potential should strongly affect the secondary electron emission current because it is equivalent to the variation of a crystal work function. The effect may be interpreted as a ''voltage contrast.''[19] Obviously the charge $\Delta\rho$ is quasiuniform over the sample surface and it does not depend on the domain orientation. Calculations of the surface potential arising from the primary beam irradiation are based on the assumption that the charge crystal bulk (interaction volume) represents a homogeneously charged cylinder of radius R (R is an electron-beam radius) and height h (h is a penetration depth of the beam). The value of R in our experimental conditions was $R \approx 0.5$ μm. The penetration depth may be estimated according to the expression[18] known as the Kanaya-Okayama range:

$$h = \frac{0.0276 A E_{\mathrm{pr}}^{1.67}}{Z^{0.89} d}, \tag{1}$$

where A is an atomic weight in g/mole, d is a density in g/cm^3, and Z is an atomic number (the beam is incident at a right angle to a sample surface). Substituting the parameters known for KTP data:[1,22] $A = 197.97$ g/mole, $Z = 14.656$, $d = 3.02$ g/cm^3, $E_{\mathrm{pr}} \approx 1$ keV, one can estimate that $h \cong 1.7 \times 10^{-5}$ cm. To calculate the bulk charge density ρ_{in} one can assume that the irradiated cylinder is charged uniformly and ρ_{in} may be written in accordingly[23]

$$\rho_{\mathrm{in}} = \frac{I_b t_a}{\pi R^2 h}, \tag{2}$$

where I_b is the primary beam current, t_a is the time of irradiation. Expression (2) has been obtained under the assumption that the injected charge is totally absorbed. Also, ρ_{in} should depend on the magnitude of the secondary-electron emission coefficient δ and expression (2) should be corrected as follows:

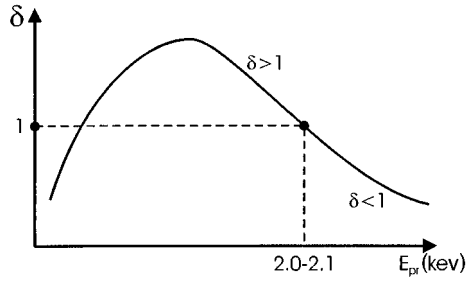

FIG. 3. Secondary-electron emission coefficient δ versus energy of the primary beam E_{pr} for the studied KTP crystal.

$$\rho_{\mathrm{in}} = \frac{I_b t_a}{\pi R^2 h}(\delta - 1). \tag{2'}$$

The value of t_a can be estimated from the expression[23]

$$t_a = \frac{t_L 2R}{L}, \tag{3}$$

where L is the length of one line scanned on the specimen and t_L is the line scanning time.[23] We estimate from the experimental conditions that $t_a \cong 1.85 \times 10^{-8}$ s and, for the primary electron current $I_b = 1.5 \times 10^{-8}$ A, $\rho_{\mathrm{in}} = 2.078 \times 10^{-3}(\delta - 1)$ C/cm^3. The surface potential U_c of this charged cylinder has been calculated from the following formula:

$$U_c = \frac{1}{4\pi\varepsilon\varepsilon_0} \oint_V \frac{\rho_{\mathrm{in}}}{r} d\nu, \tag{4}$$

where ε is the dielectric permittivity and r is the coordinate. The solution of (4) gives

$$U_c = \frac{\rho_{\mathrm{in}}}{4\varepsilon\varepsilon_0}\left[h\sqrt{h^2 + R^2} + R^2 \ln\left(\frac{h + \sqrt{h^2 + R^2}}{R}\right) - h^2 \right]. \tag{5}$$

The estimated surface potential appeared due to the irradiation by the primary beam is, thus, $U_c \approx 170(\delta - 1)$ mV. Variation of the potential U_c depends on the δ value. The dependence $\delta(E_{\mathrm{pr}})$ is identical for all kinds of materials (Fig. 3).[18,19] We have gauged the value of E_{pr} in accordance with the method[15] when the secondary-electron emission coefficient $\delta = 1$. For the studied KTP crystals $\delta = 1$ was observed for $E_{\mathrm{pr}} \approx 2.0$–$2.1$ kV. Exactly at this energy the drastic changes of the contrast behavior has been observed (Figs. 1 and 2). Implemented measurements of δ make it possible to define the sign of potential U_c. Obviously, for $E_{\mathrm{pr}} > 2.0$ kV, $\delta < 1$, and U_c is negative, while at low voltages, $E_{\mathrm{pr}} < 2.0$ kV, $\delta > 1$ (Fig. 3), and the surface potential is positive, $U_c > 0$. Unfortunately, quantitative data on δ values are very limited for ferroelectrics and they are unknown for KTP. In Ref. 24 the coefficient δ was gauged in $LiNbO_3$. The maximum value of δ was $\delta_{\max} \cong 1.8$ at $E_{\mathrm{pr}} \approx 400$ eV and $\delta(E_{\mathrm{pr}})$ curve decayed slowly for $\delta > 1$.

The second reason for the surface potential changes is a pyroelectric potential U_{pyro} that appears due to the specimen heating by absorbed electrons. Estimation of the temperature change $\Delta\theta$ for any material subjected to the electron irradiation in SEM was done in Ref. 23. The authors showed that for insulators $\Delta\theta$ is as follows:

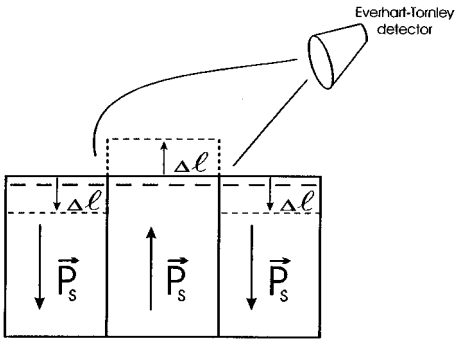

FIG. 4. Scheme of the appearance of the boundary contrast in the KTP crystal ($E_{pr}>2.1$ keV).

$$\Delta\theta=\frac{I_b E_{pr} t_a}{4.186\pi a^2 hdc}, \tag{6}$$

where c is the specific heat. For KTP crystals $c=0.174$ cal/g °C (Ref. 1) and expression (6) gives $\Delta\theta\cong 0.96$ °C.

Having $\Delta\theta$ and estimated sizes of the irradiated volume of the crystal one can calculate the pyroelectric potential:

$$U_{pyro}=\frac{\gamma\Delta\theta h}{\varepsilon\varepsilon_0}, \tag{7}$$

where γ is the KTP pyroelectric coefficient. According to Ref. 1 for KTP crystals $\gamma=7\times10^{-9}$ C cm^{-2} K^{-1} and $U_{pyro}\approx 240$ mV. The sign of a pyroelectric potential at a polar surface is defined by the direction of a spontaneous polarization $\mathbf{P}_s$. Heating a ferroelectric specimen by an electron beam causes $U_{pyro}<0$ for C^+ domains and $U_{pyro}>0$ for C^- domains.

VI. ORIGIN OF DOMAIN AND BOUNDARIES CONTRAST IN SEM

The resulting potential U of the irradiated surface is the algebraic sum of the pyroelectric potential U_{pyro} and the uniform surface potential U_c appearing under the electron-beam irradiation. Both potentials are associated with electrostatic charges. Generation of charges in ferroelectric-semiconductor crystal causes their screening. The characteristic time of the screening process is the Maxwell relaxation time, $\tau_m=\varepsilon\varepsilon_0/\sigma$, where σ is the crystal conductivity. Our measurements of KTP specimens used show that $\sigma_{zz}\approx 2.6\times10^{-8}$ Ω^{-1}cm^{-1}. For the known $\varepsilon=20$, $\tau_m\approx 6.8\times10^{-5}$ s. The appearing charges are screened in accordance with the simple equation $\rho=\rho_0\exp(-t_a/\tau_m)$. The time of irradiation t_a estimated above [expression (3)] is $t_a=1.85\times10^{-8}$ s which is much less than τ_m. It means that the charges induced by the primary beam and pyroelectric charges are not relaxed sufficiently in the used TV scanning mode ($t_a\ll\tau_m$). One can assume that there is a strong influence of this charging process on the observed domain contrast.

Electron-beam irradiation in the region $\delta>1$ ($E_{pr}<2.0$ kV, Fig. 3) causes the appearance of uniformly distributed positive charges [the potential $U_c=170(\delta-1)$ mV]. The pyroelectric potentials [expressions (6) and (7)] for a C^+ domain will be $U_{pyro}\cong -240$ mV and for C^- domain $U_{pyro}\cong +240$ mV.

The resulting surface potentials for these domains may be defined as

$$U_{C^+}=-U_{pyro}+U_c,$$

$$U_{C^-}=U_{pyro}+U_c. \tag{8}$$

Equation (8) shows that in the low-voltage regime ($E_{pr}<2.0$ keV) $\delta>1$ and the resulting potential of the C^- domain is always positive $U_{C^-}>0$. The potential for the C^+ domains depends on the δ value. As mentioned above, δ_{max} for $LiNbO_3$ was equal $\delta=1.8$. If we assume that $\delta_{max}\sim 2$ one can obtain that the resulting potential for the C^+ domains is negative, $U_{C^+}<0$. Obviously, changes of the surface potential causes a work function decrease for C^+ domains and its increase for C^- domains. The work function difference is $\Delta A=U_{C^-}-U_{C^+}=2U_{pyro}$ and it is about $\Delta A\cong 0.5$ eV. Our measurements of the work function for the equilibrium state show that $A_{C^+}\approx A_{C^-}\approx 4.5$ eV. Taking into account the value of energy gap for KTP (Ref. 1) $E_g=3.5$ eV, one can get the electron affinity $\xi=1$ eV. The pyroelectrically induced difference in the domain work function is derived from Eq. (8) as $\Delta A\cong 0.5$ eV. This value is about 50% from the measured electron affinity. It means that the pyroelectric contrast is the dominant reason.

These estimates make it possible to interpret the domain contrast as follows. Electron irradiation of the ferroelectric surface causes the appearance of asymmetric fluxes of the secondary electrons when $J_{C^+}>J_{C^-}$. Electron escape from the surface is also asymmetric because the resulting work function for C^+ domains is sufficiently smaller than for C^- domains. Both reasons should lead to difference in the secondary-electron emission from opposite sign domains. This conclusion is consistent with the experimental data (Fig. 2) when C^+ domains are bright and C^- domains look darker.

In the regime when $E_{pr}>2.0$ keV and $\delta<1$ the domain boundary contrast is observed only (Fig. 1). The potential U_c has a negative value while the signs of U_{pyro} for the C^- and C^+ domains remains unchanged:

$$U_{C^+}=-U_{pyro}-U_c,$$

$$U_{C^-}=U_{pyro}-U_c. \tag{9}$$

Figure 1 demonstrates the complete disappearance of the domain contrast. Probably the reason for this might be explained as follows. Enhancement of the value of beam energy E_{pr} causes an increase in the penetration depth h and reduces the local heating $\Delta\theta$. As a result, the influence of the pyroelectric potential on the domain contrast becomes smaller. In this case the dominant charge will be the uniform negative charge induced by the primary beam.

However, the domain boundary contrast arises (Fig. 1). It should be noted that both images [Figs. 1(a) and 1(b)] illustrate the same feature: the left boundaries are dark and the right ones are bright. As it has been described the SEM image presented in Fig. 1(b) was obtained when the KTP specimen was turned around Z axis by 180° with respect to the sample orientation corresponding to Fig. 1(a). The Everhart-

Tornley detector of the secondary electrons is situated on the right-hand side of the sample (Fig. 4). This means that the electron detector does not ''see'' the left side of the C^+ domain and it does ''see'' the right. One can suggest that it may occur due to the lifting of C^+ domains and to the lowering of the C^- domains. Charging of any ferroelectric crystal causes the appearance of the converse piezoelectric effect. It leads to the elastic deformation Δl of the crystal. The sign of the deformation Δl is opposite for the different domains (Fig. 4) when they are charged identically. For the same negative charges injected by the primary beam Figs. 1(a) and 1(b) demonstrate the strong boundary contrast and one can assume that the contrast may occur due to the converse piezoelectric effect. We believe that the obtained data may be used for observation of a domain grating in KTP nonlinear optical devices.

VII. CONCLUSIONS

(1) The domain and boundary contrasts are observed in as-grown KTP crystals by the SEM method. (2) Two quite different types of the contrast have been revealed. It is shown that in the TV scanning mode and for $\delta>1$ the domain contrast is caused by opposite pyroelectric potentials for C^+ and C^- domains. The boundary contrast is of topographic origin. We attribute it to the converse pieozoelectric effect in the regime when the secondary-electron emission coefficient $\delta<1$.

ACKNOWLEDGMENT

The authors are grateful to Dr. L. Burstein for the work-function measurements.

*Electronic address: gilr@eng.tau.ac.il

[1] J. D. Beirlein and H. Vanherzeele, J. Opt. Soc. Am. B **6**, 622 (1989).
[2] L. K. Cheng and J. D. Beirlein, Ferroelectrics **142**, 209 (1993).
[3] J. D. Beirlein, D. B. Laubacher, J. B. Brown, and C. J. van der Poel, Appl. Phys. Lett. **56**, 1729 (1990).
[4] D. Eger, M. Oron, M. Katz, and A. Zussman, Appl. Phys. **77**, 2205 (1995).
[5] J. C. Burfoot and G. W. Taylor, *Polar Dielectrics and Their Applications* (University of California Press, Berkeley, 1979).
[6] R. Lüthi, H. Haefke, K.-P. Meyer, E. Meyer, L. Howald, and H.-J. Güntherodt, J. Appl. Phys. **74**, 7461 (1993).
[7] J. D. Beirlein and F. Ahmed, Appl. Phys. Lett. **51**, 1322 (1987).
[8] F. Laurell, M. G. Roefols, M. Bindloss, H. Hsuing, A. Suna, and J. D. Beirlein, J. Appl. Phys. **71**, 4664 (1992).
[9] N. R. Ivanov, N. A. Tikhomirova, A. V. Grinzberg, S. P. Chumakova, E. I. Eknadiosyants, V. Z. Borodin, A. N. Pinskaya, V. A. Babonskikh, and V. A. Dyakov, Crystallogr. Rep. **39**, 593 (1994).
[10] N. Angert, L. Kaplun, M. Tseitlin, E. Yashin, and M. Roth, J. Crystal Growth **137**, 116 (1994).
[11] Q. Chen and W. P. Risk, Electron. Lett. **30**, 1516 (1994).
[12] R. Le Bihan and C. Sella (unpublished).
[13] R. Le Bihan and M. Maussion, C. R. Acad. Sci. **272B**, 1010 (1971).
[14] M. Maussion and R. Le Bihan, Ferroelectrics **13**, 465 (1976).
[15] R. Le Bihan, Ferroelectrics **97**, 19 (1989).
[16] V. Aristov and L. Kokhanchik, Ferroelectrics **126**, 353 (1992).
[17] A. Sogr, Ferroelectrics **97**, 47 (1989).
[18] J. I. Goldstein, *Scanning Electron Microscopy and X-Ray Microanalysis* (Plenum, New York, 1992).
[19] *SEM Microcharacterization of Semiconductors*, edited by D. B. Holt and D. C. Joy (Academic, London, 1989).
[20] B. I. Sturman and V. M. Fridkin, *The Photovoltaic and Photorefractive Effect in Nonsymmetric Materials* (Gordon and Breach, Philadelphia, 1992).
[21] A. M. Glass, D. von der Linde, and I. J. Negran, Appl. Phys. Lett. **25**, 233 (1974).
[22] V. Voronkova, S. Yu. Stefanovich, and V. K. Yanovski, Sov. J. Quant. Electron. **16**, 480 (1988).
[23] K. Kanaya and S. Ono, *Electron Beam Interactions with Solids* (SEM, O'Hare, Chicago, 1984).
[24] M. N. Deviatkov, V. I. Ktitorov, and Yu. I. Samsonov, Sov. Phys. Izv. **40**, 2604 (1976).